Conference on Modelling Fluid Flow (CMFF'22)
The 18th International Conference on Fluid Flow Technologies
Budapest, Hungary, August 30-September 2, 2022

Numerical study of vortex-induced vibration of a circular cylinder subject to oscillatory flow at high Keulegan-Carpenter numbers

Dániel DOROGI[1], Efstathios KONSTANTINIDIS[2], László BARANYI[3]

[1] Corresponding Author. Department of Fluid and Heat Engineering, Institute of Energy Engineering and Chemical Machinery, Faculty of Mechanical Engineering and Informatics, University of Miskolc. H-3515 Miskolc-Egyetemváros. Tel.: +36 46 565 111, E-mail: daniel.dorogi@uni-miskolc.hu
[2] Department of Mechanical Engineering, University of Western Macedonia, Greece. E-mail: ekonstantinidis@uowm.gr
[3] Department of Fluid and Heat Engineering, Institute of Energy Engineering and Chemical Machinery, Faculty of Mechanical Engineering and Informatics, University of Miskolc, Hungary. E-mail: laszlo.baranyi@uni-miskolc.hu

ABSTRACT

This work investigates the vortex-induced vibration of a circular cylinder placed perpendicular to a uniform oscillatory flow at the Keulegan-Carpenter number values of 500, i.e. in the drag-dominated regime. The cylinder was allowed to vibrate in the direction transverse to the oscillatory flow. The non-dimensional forms of the governing equations for fluid flow and cylinder motion were solved in a non-inertial reference frame using an in-house finite-difference code. Simulations were conducted for a system with mass ratio of 2 with zero structural damping. The maximum Reynolds number and maximum reduced velocity are set to 150 and 5, respectively. It is shown that the cylinder response comprises high-frequency vortex-induced vibrations and low-frequency wave-induced oscillations. Plots of the phase-averaged vibration amplitude and fluid force as functions of the time-dependent reduced velocity display strong hysteresis. It is further shown that the phase-averaged amplitude over the deceleration stage follows quite closely the path traced by data points from steady-flow tests. However, the fluid forces that drive the motion are markedly different over a large part of the time-dependent reduced velocity domain for oscillatory and steady flows.

Keywords: drag-dominated range, Keulegan-Carpenter number, oscillatory flow, vortex-induced vibration

NOMENCLATURE

$\mathcal{D}$	[−]	dilation, non-dimensionalised by U_m/D
A^*	[−]	vibration amplitude non-dimensionalised by D
$C_{x,y}$	[−]	magnitudes of non-dimensional fluid forces in x and y directions
D	[m]	cylinder diameter
$F^*_{x,y}$	[−]	fluid forces in x and y directions non-dimensionalised by $\frac{1}{2}\rho U_m^2 D$
K_C	[−]	Keulegan-Carpenter number, $K_C = U_m/(f_o D)$
R	[−]	radius non-dimensionalised by D
Re	[−]	Reynolds number, $U_m D/\nu$
U	[−]	velocity of the uniform stream non-dimensionalised by U_m
U_m	[−]	magnitude of the stream velocity
U_r	[−]	reduced velocity, $U_m/(f_n D)$
c	[kg/s]	structural damping
f_n	[s^{-1}]	natural frequency of the cylinder in vacuum
f_o	[s^{-1}]	frequency of the uniform stream
f^*_y	[−]	vibration frequency non-dimensionalised by U_m/d
$f^*_{C_{x,y}}$	[−]	frequencies of fluid forces in x and y directions non-dimensionalised by U_m/d
k	[N/m]	spring stiffness
m	[kg/m]	mass of the cylinder per unit length
p	[−]	pressure non-dimensionalised by ρU_m^2
t	[−]	time non-dimensionalised by D/U_m
$u,\ v$	[−]	velocities in x and y directions non-dimensionalised by U_m
$x,\ y$	[−]	Cartesian coordinates non-dimensionalised by D
y_c	[−]	cylinder displacement non-dimensionalised by D

μ	[−]	mass ratio, $4m/(\rho D^2\pi)$
ν	[m^2/s]	kinematic viscosity of the fluid
ρ	[kg/m^3]	fluid density
ζ	[−]	structural damping ratio, $c/(2\sqrt{km})$

Subscripts and Superscripts

1, 2	on the cylinder surface, at the outer boundary of the domain
c	refers to cylinder response (y_c)
x, y	streamwise, transverse
$\widetilde{\dots}$	dimensional quantity ($\widetilde{U}$)

1. INTRODUCTION

Vortex-induced vibration (VIV) of bluff structural elements is a practical fluid-structure interaction (FSI) mechanism playing a significant role for example in offshore platforms, risers, offshore wind turbines or high slender buildings. Due to its importance, this phenomenon has been thoroughly investigated in the past decades using both laboratory experiments and numerical simulations; the most significant review papers are Bearman [1, 2], Sarpkaya [3] and Williamson and Govardhan [4].

The majority of the FSI researches have investigated the case of an elastically supported circular cylinder placed into a uniform free stream [5, 6, 7]. However, engineering structures are often exposed to waves; FSI studies on waves include [8, 9, 10]. Waves are usually modelled using a uniform oscillatory flow, where the velocity of the stream can be written as $\widetilde{U}(t) = U_m \sin(2\pi f_o t)$, where t is the time, U_m and f_o are the magnitude and frequency of the stream velocity, respectively. The Keulegan-Carpenter number $K_C = U_m/(f_o D)$ and the Reynolds number $Re = U_m D/\nu$ are the dimensionless groups used to characterise the incoming stream, where D is the cylinder diameter and ν is the kinematic viscosity of the fluid.

In VIV, generally the cylinder can move in two directions, i.e. streamwise with and transverse to the free stream [10, 11]. However, researchers often consider one-degree-of-freedom cylinder motion. Williamson [8] constructed an analytical approach to predict streamwise-only VIV of a circular cylinder. The author solved the equation of cylinder motion together with Morison *et al*. [12]'s formulation for the streamwise fluid force. Williamson [8] found that the predicted response compares well with experimental results. Anagnostopulos and Illiadis [13] and Taheri *et al*. [14] investigated a similar problem using two-dimensional (2D) computational fluid dynamics (CFD) simulations.

Transverse-only vortex-induced vibrations have been found to be more important, because the oscillation amplitudes are higher in this directions than those in the streamwise direction. Sumer and Fredsøe [9] experimentally investigated the VIV of a circular cylinder in the Keulegan-Carpenter number range of $K_C = 5 - 100$. They showed that when increasing K_C above 5 the cylinder undergoes high-amplitude vibrations with the amplitude depending on the value of the reduced velocity $U_r = U_m/(f_n D)$, where f_n is the natural frequency of the cylinder in vacuum. In contrast to the VIV response in a uniform free stream, lock-in/synchronisation occurs over several 'sections' in the U_r domain. McConnel and Jiao [15] observed similar characteristics in their experimental results. Zhao *et al*. [16] carried out extensive 2D simulations for $K_C = 10$ and 20. They found that in the reduced velocity domain of $U_r < 8$ the frequency spectra of cylinder displacement contains one dominant peak at twice the flow oscillation frequency. However, above $U_r = 8$ Zhao *et al*. [16] identified multiple peaks, which are the whole number multiples of the frequency of the main stream. Zhao *et al*. [17] found similar features, i.e. multiple frequency peaks in the cylinder response, using three-dimensional computations.

The studies mentioned above have been limited to low Keulegan-Carpenter number values, i.e. $K_C < 100$; no results exist at high K_C values. In this study transverse-only VIV of a circular cylinder placed into an oscillatory flow is investigated at the high Keulegan-Carpenter number value of $K_C = 500$ by means of 2D finite-difference computations. The maximum reduced velocity, maximum Reynolds number, mass ratio and structural damping ratio values are fixed at $U_r = 5, Re = 150, \mu = 2$ and $\zeta = 0$, respectively. Since the difference between K_C and U_r is large, the cylinder response might be expected to be strongly modulated. The main objective of this study is to develop a methodology to analyse the oscillation amplitude and frequency and fluid forces acting on the cylinder.

2. METHODOLOGY

The two-dimensional flow of the Newtonian incompressible constant property fluid is governed by the two components of the Navier-Stokes equations written in a non-inertial reference frame attached to the vibrating cylinder, the continuity equation and the pressure Poisson equation. The non-dimensional forms of these equations are written as follows:

$$\frac{\partial u}{\partial t} + u\frac{\partial u}{\partial x} + v\frac{\partial u}{\partial y} = -\frac{\partial p}{\partial x} + \frac{1}{Re}\nabla^2 u + \dot{U}, \tag{1}$$

$$\frac{\partial v}{\partial t} + u\frac{\partial v}{\partial x} + v\frac{\partial v}{\partial y} = -\frac{\partial p}{\partial y} + \frac{1}{Re}\nabla^2 v - \ddot{y}_c, \tag{2}$$

$$\mathcal{D} = \frac{\partial u}{\partial x} + \frac{\partial v}{\partial y} = 0, \tag{3}$$

$$\nabla^2 p = 2\left(\frac{\partial u}{\partial x}\frac{\partial v}{\partial y} - \frac{\partial u}{\partial y}\frac{\partial v}{\partial x}\right) - \frac{\partial \mathcal{D}}{\partial t}, \tag{4}$$

where t is the dimensionless time, x and y are the non-dimensional Cartesian coordinates in the streamwise and transverse directions, respectively, u and v are the non-dimensional streamwise and transverse velocity components of the fluid, p is the non-

dimensional pressure, $\mathcal{D}$ is the dilation and $\ddot{y}_c$ is the non-dimensional acceleration of the cylinder in the transverse direction. In this study the cylinder diameter D and the magnitude of the stream velocity U_m are used as length and velocity scales, respectively. Although the dilation is zero by Eq. (3), $\partial\mathcal{D}/\partial t$ is kept in Eq. (4) to reduce numerical errors [18]. In Eq. (1) $U = \sin(2\pi t/K_C)$ is the non-dimensional velocity of the fluid stream, where $K_C = U_m/(f_o D)$ is the Keulegan-Carpenter number based on the flow oscillation frequency f_o. In Eqs. (1) and (2) $Re = U_m D/\nu$ is the maximum Reynolds number, where ν is the kinematic viscosity of the fluid, and in these equations the overdot represents differentiation with respect to time. The transverse acceleration component of the cylinder in Eq. (2) is obtained by solving Newton's second law of cylinder motion. This equation in non-dimensional form is written as follows:

$$\ddot{y}_c + \frac{4\pi\zeta}{U_r}\dot{y}_c + \left(\frac{2\pi}{U_r}\right)^2 y_c = \frac{2}{\pi\mu}F_y^*(t), \qquad (5)$$

where y_c, $\dot{y}_c$ and $\ddot{y}_c$ are the non-dimensional cylinder displacement, velocity and acceleration, respectively, $U_r = U_m/(f_n D)$ is the maximum reduced velocity, where f_n is the natural frequency of the cylinder in vacuum, ζ and μ are the structural damping ratio and the mass ratio, respectively, and $F_y^*(t)$ is the non-dimensional sectional fluid force acting on the cylinder.

The physical domain of the computations is considered to be an area confined between two concentric circles: R_1 is the non-dimensional radius of the cylinder surface, while R_2 is that of the outer surface. On $R = R_1$ no-slip boundary conditions are applied for u and v, while for the fluid pressure a Neumann-type condition is used. On $R = R_2$, the pressure gradient is set to zero, while the two velocity components are chosen to be $u = U(t)$ and $v = -\dot{y}_c(t)$.

In order to achieve high degree of accuracy the physical domain is transformed to a computational domain on which an equidistant grid is generated; the mesh is boundary-fitted on the physical plane [19]. The transformed governing equations with boundary conditions are solved using an in-house CFD code based on the finite difference method [19, 7, 20]. The spatial derivatives are approximated using fourth-order accurate central difference schemes except for the convective terms, which are discretised by applying a modified third-order upwind difference scheme. Eqs. (1) and (2) are integrated with respect to time using the explicit Euler approach, while the fourth-order explicit Runge-Kutta method is implemented for the time discretisation of Eq. (5). The successive over-relaxation method is used to solve the linear system resulting from the discretisation of the pressure Poisson equation while satisfying the continuity equation in each time step.

The number of grid points in the peripheral and radial directions are set to 361 and 314, respectively,

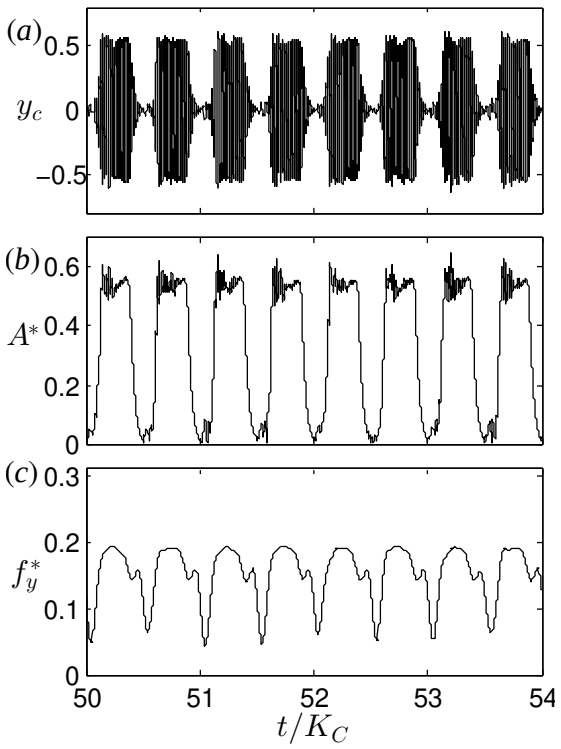

Figure 1. Time histories of (a) cylinder displacement y_c, (b) amplitude A^* and (c) frequency f_y^* of cylinder oscillation

the radius ratio R_2/R_1 is chosen to be 240 and the dimensionless time step is fixed at $\Delta t = 0.0005$. The currently applied CFD code has been extensively validated against data in the literature for stationary cylinder, forced cylinder oscillation and vortex-induced vibration cases [19, 7, 20].

3. RESULTS AND DISCUSSION

In this study two-dimensional CFD computations are carried out in order to investigate vortex-induced vibrations of a circular cylinder placed into the high-Keulegan-Carpenter-number (and thus slowly-varying) oscillatory flow of $K_C = 500$. The maximum Reynolds number, maximum reduced velocity and mass and structural damping ratio values are fixed at $Re = 150$, $U_r = 5$ $\mu = 2$ and $\zeta = 0$, respectively. Figure 1 shows the non-dimensional cylinder displacement y_c and its amplitude A^* and frequency f_y^* against time. Note that time histories in this and subsequent figures correspond to the time interval $t/K_C = 50 - 54$, i.e. over 4 periods of the oscillatory flow. The cylinder displacement displays intervals of high-amplitude between intervals of low-oscillation amplitude in each flow cycle (see Fig. 1a). By applying the Hilbert transform [6] to the displacement signal it is possible to obtain the time-dependent amplitude and frequency of the cylinder, shown in Fig. 1b and 1c, respectively. As can be seen in Fig. 1b the time-dependent amplitude varies approximately between zero and 0.6. The maximum value is close

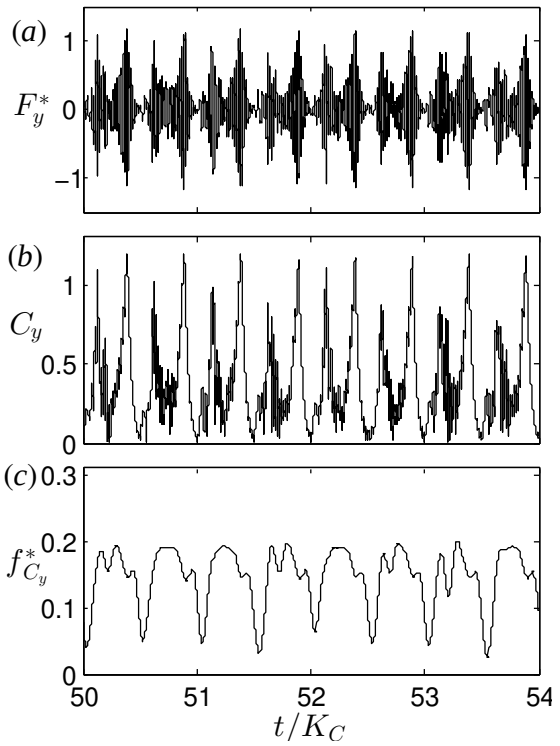

Figure 2. Time histories of (*a*) transverse fluid force F_y^*, (*b*) and magnitude C_y and (*c*) frequency $f^*_{C_y}$ of F_y^*

to the peak amplitude of transverse response in uniform free stream at low Reynolds numbers in the unsteady laminar regime [21, 22]. As shown in Fig. 1*c*, the time-dependent vibration frequency varies from a minimum value of approximately 0.05 up to 0.20. The maximum value (i.e. 0.2) corresponds to the reciprocal of the maximum reduced velocity U_r^{-1}. It is interesting to note that neither $A^*(t)$ nor $f_y^*(t)$ displays smooth harmonic-like variations (see discussion of phase-averaging below).

Figure 2 shows the time histories of the transverse fluid force F_y^*, i.e. the motion-driving force, and the magnitude C_y and frequency $f^*_{C_y}$ of the force signal obtained using the Hilbert transform. As can be seen Fig. 2*b*, the time-dependent magnitude of F_y^* fluctuates between a minimum value of approximately zero and a maximum value slightly above 1.0. It might be noted that fluctuations in the time-dependent force magnitude occur at four times the frequency of flow oscillation due to peaking twice each time the flow speed increases either in the positive or the negative direction. Despite being essentially periodic, fluctuations in $C_y(t)$ have rather stochastic cycle-to-cycle variations, which are also evident in the time history of its frequency $f^*_{C_y}(t)$ (see Fig. 2*c*).

Figure 3 shows the frequency of the driving force against the frequency of cylinder vibration in the time interval $50K_C \leq t \leq 54K_C$, i.e. the period analysed

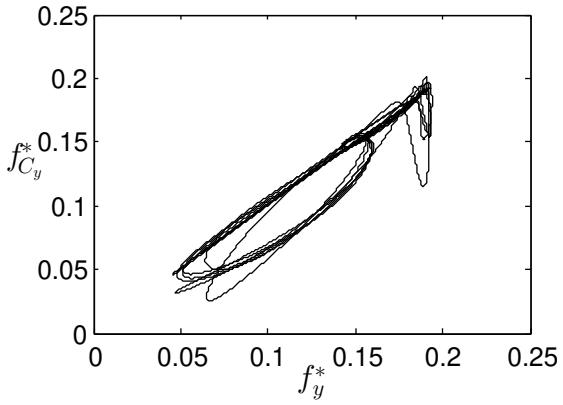

Figure 3. Time-dependent frequency of cylinder vibration against the frequency of transverse fluid force within the non-dimensional time interval $50K_C \leq t \leq 54K_C$

in Figs. 1 and 2. It can be seen that the driving force and the cylinder have the same frequency over part of the flow oscillation. However, $f^*_{C_y}(t)$ and $f_y^*(t)$ are different over another part of the flow oscillation; the elliptical-like trajectory suggests that there is a definite relationship between them. In addition, there also exist deviations from the elliptical-like trajectory, which might be attributed to the stochastic cycle-to-cycle variations in the behaviour of the system.

Figure 4*a* shows the time history of the fluid force acting in the direction of the main flow. The streamwise fluid force F_x^* displays fluctuations in the period of flow oscillation and overriding high-frequency fluctuations that appear at intervals near its peak magnitude. The low- and high-frequency fluctuations are separated from each other using a low-pass filter in order to analyse the streamwise force more thoroughly. The low-frequency force component F^*_{xf} shown in Fig. 4*b* displays very repeatable oscillations. This component can be modelled very accurately using Morison *et al.*'s equation [12] but this is not explored further here.

The high-frequency component is obtained by subtracting the low-frequency component from the total force $F_x^* - F^*_{xf}$ and the resulting signal is shown in Fig. 4*c* (black line). Then, the time-dependent magnitude $C_x(t)$ and frequency $f^*_{C_x}(t)$ of the streamwise force are obtained by applying the Hilbert transform to the high-frequency signal. The resulting time histories are plotted in Fig. 4*c* (red line) and 4*d*, respectively. It can be seen in Fig. 4*c* that $C_x(t)$ displays a variation similar to that of $A^*(t)$, i.e. intervals of high amplitudes interspersed intervals of low-amplitude. As can be seen in Fig. 4*d*, the maximum of $f^*_{C_x}$ is approximately 0.4, which is roughly the twice the peaks of f_y^* or $f^*_{C_y}$ (see Figs. 1*c* and 2*c*). This finding is consistent with the results from VIV in uniform free stream; in those cases the frequency of the F_x^* is always twice the frequency of F_y^* [21].

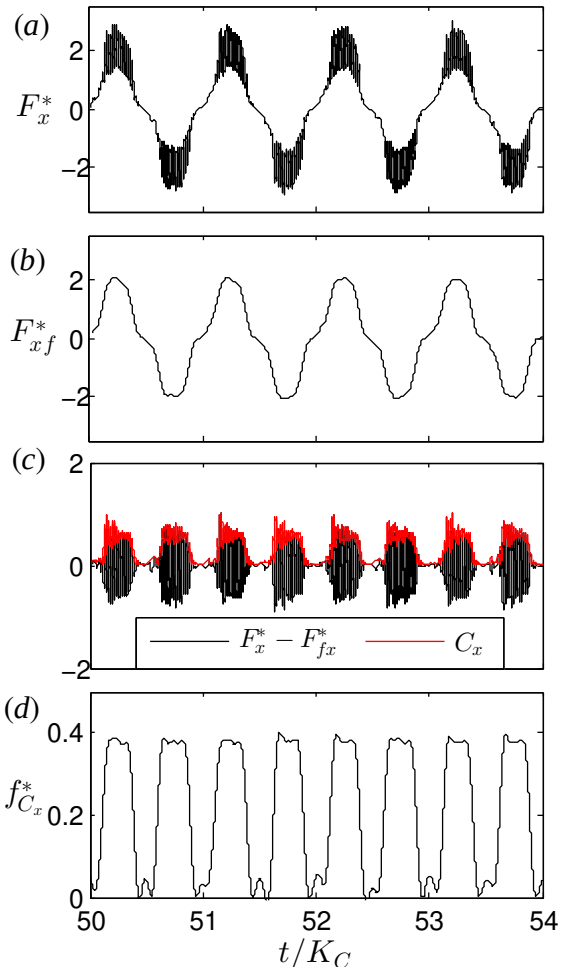

Figure 4. Time histories of (*a*) streamwise fluid force F_x^*, (*b*) low-frequency component of force F_{xf}^*, (*c*) high-frequency component of F_x^* and its magnitude C_x and (*d*) frequency of the high-frequency force component $f_{C_x}^*$

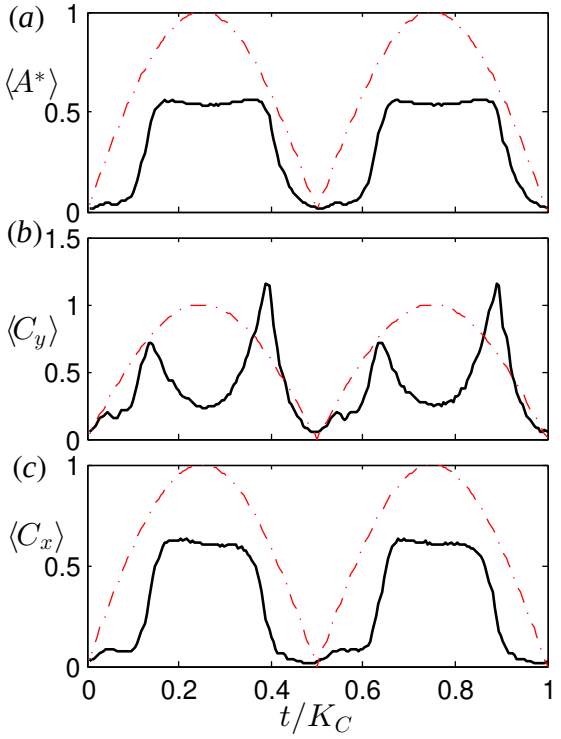

Figure 5. Phase-averaged (*a*) amplitude of cylinder displacement, (*b*) transverse fluid force and (*c*) streamwise fluid force. The red dashed line represents $|U(t)|$.

In addition, it is interesting to note that the minimum value of $f_{C_x}^*$ is approximately zero; this contrasts with the variation of $f_{C_y}^*$ (see Fig. 2*c*).

The displacement and force signals over 100 flow cycles were phase averaged using 200 non-overlapping bins, each containing 5000 data points. Phase-averaged results for the response amplitude $\langle A^* \rangle$ are shown in Fig. 5*a*. It can be seen that the amplitude response is high during the part of high-speed flow. Remarkably, $\langle A^* \rangle$ increases and decreases much more abruptly than the flow speed and attains two local maxima; one during the flow deceleration stage ($t/K_C = 0 - 0.25$) and another during the flow acceleration stage ($t/K_C = 0.25 - 0.5$). These local maxima are accompanied by marked increases in the phase-averaged magnitude of the transverse force $\langle C_y \rangle$, as can be seen in Fig. 5*b*. During the deceleration stage the driving force leads the motion, whereas force and motion are almost in phase during the acceleration stage. Furthermore, the local peak in $\langle C_y \rangle$ is much higher (nearly double) during the acceleration stage than during the deceleration stage. These observations signify fundamental differences in the mechanisms related to flow-induced vibration during different parts of the flow-oscillation cycle. On the other hand, the variation of the phase-averaged magnitude of the streamwise force $\langle C_x \rangle$ is very similar to that of $\langle A^* \rangle$, as can be seen in Fig. 5*c*.

Additional simulations are conducted for the case when the cylinder is placed into a uniform free stream. For simplicity we will refer to this case as 'steady-VIV'. The parameters of these computations (i.e. the Reynolds number and reduced velocity) are chosen so as to correspond to the conditions at selected points of the oscillatory flow. Figure 6 provides comparisons of the phase-averaged results in oscillatory flow against steady-VIV data. It can be seen that the time-dependent amplitude response over the deceleration stage in oscillatory flow (see red curves in Fig. 6) follows quite closely the path traced by the steady-VIV amplitude as a function of the time-dependent reduced velocity $U_r^*(t) = \widetilde{U}/(f_n D)$. At the peak reduced velocity (i.e. $U_r^*(t) = U_r$), results for both oscillatory-VIV and steady-VIV almost coincide, including the magnitude of the fluid forces. However, during the acceleration stage (blue), the response amplitude is markedly higher in oscillatory-VIV than in steady-VIV and a hysteresis loop is formed in the plot of $\langle A^* \rangle$ as a function of $U_r^*(t)$.

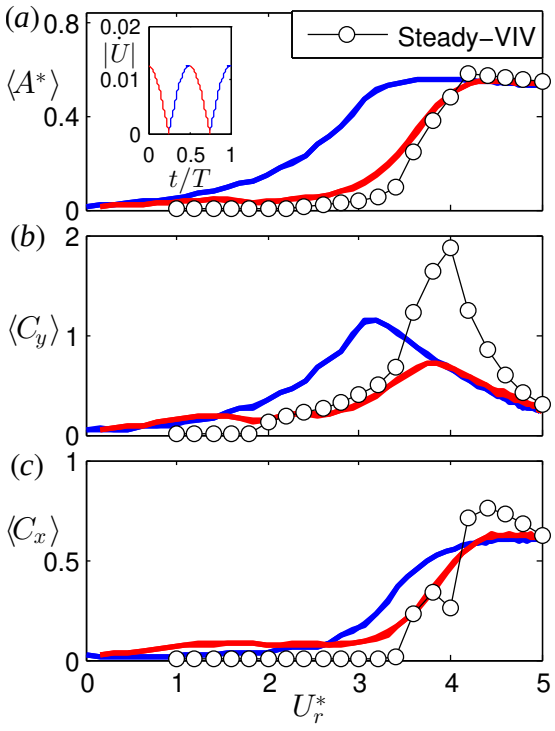

Figure 6. Comparison of results for oscillatory-VIV (coloured lines) with corresponding steady-VIV data (black circles+lines). The insert shows the stages of flow acceleration (blue) and deceleration (red) in absolute values for oscillatory-VIV

Similar trends can be observed in the variation of the magnitude of the unsteady fluid forces (high-frequency components). Furthermore, it is interesting to observe the marked differences in the magnitude of the transverse force near $U_r^*(t) = 4$, where $\langle C_y \rangle$ for steady-VIV is more than twice its value for oscillatory-VIV, despite the fact that the amplitude is almost the same for both cases.

4. CONCLUSIONS

In this study vortex-induced vibrations of a circular cylinder placed into a high-Keulegan-Carpenter-number (i.e. $K_C = 500$) oscillatory flow is investigated by means of two-dimensional finite-difference simulations. The maximum Reynolds number, the maximum reduced velocity and the mass and structural damping ratios are fixed at the values of $Re = 150$, $U_r = 5$, $\mu = 2$ and $\zeta = 0$, respectively.

The time-dependent magnitude and frequency of the signals (i.e. cylinder displacement and fluid forces) are obtained from Hilbert transform of the high-frequency (filtered) signals. The oscillation amplitude and the magnitude of the streamwise fluid force follow similar trends: in each flow oscillation cycle a time interval of high amplitudes is between intervals of low-amplitudes. In contrast, the magnitude of the transverse fluid force fluctuates at twice the frequency of the oscillation amplitude. The maximum frequency of the cylinder displacement and transverse fluid force are approximately 0.2, which is identical to the reciprocal value of the maximum reduced velocity U_r^{-1}. However, the peak frequency of the streamwise fluid force is approximately 0.4, i.e. close to the value of $2U_r^{-1}$.

Plots of the phase-averaged vibration amplitude and fluid forces (calculated based on 100 flow oscillation cycles) display strong hysteresis behaviour, which is unexpected given the very slow variation of the flow speed. This highlights the strongly nonlinear dynamics of vortex-induced vibration. The simulation results from the oscillatory flow are compared with the corresponding steady-VIV results (i.e. cases when the cylinder is placed into a uniform free stream). Although the amplitude of cylinder vibration and the magnitude of the streamwise fluid force compare relatively well, higher discrepancies are found in the magnitude of the transverse fluid force.

ACKNOWLEDGEMENTS

DD and LB was supported by the European Union and the Hungarian State, co-financed by the European Regional Development Fund in the framework of the GINOP-2.3.4-15-2016-00004 project, aimed to promote the cooperation between the higher education and the industry.

REFERENCES

[1] Bearman, P., 1984, "Vortex Shedding from Oscillating Bluff Bodies", *Annual Review of Fluid Mechanics*, Vol. 16, pp. 195–222.

[2] Bearman, P., 2011, "Circular Cylinder Wakes and Vortex-Induced Vibrations", *Journal of Fluids and Structures*, Vol. 27 (5-6), pp. 648–658.

[3] Sarpkaya, T., 2004, "A Critical Review of the Intrinsic Nature of the Vortex-Induced Vibrations", *Journal of Fluids and Structures*, Vol. 19 (4), pp. 389–447.

[4] Williamson, C., and Govardhan, R., 2004, "Vortex-Induced Vibration", *Annual Review of Fluid Mechanics*, Vol. 36, pp. 413–455.

[5] Khalak, A., and Williamson, C., 1999, "Motions, Forces and Mode Transitions in Vortex-Induced Vibrations at Low Mass-Damping", *Journal of Fluids and Structures*, Vol. 13 (7-8), pp. 813–851.

[6] Konstantinidis, E., Zhao, J., Leontini, J., Lo Jacono, D., and Sheridan, J., 2020, "Phase Dynamics of Effective Drag and Lift Components in Vortex-Induced Vibration at Low Mass–Damping", *Journal of Fluids and Structures*, Vol. 96, p. 103028.

[7] Dorogi, D., and Baranyi, L., 2020, "Identification of Upper Branch for Vortex-Induced Vibration of a Circular Cylinder at $Re = 300$", *Journal of Fluids and Structures*, Vol. 98, p. 103135.

[8] Williamson, C. H. K., 1985, "In-Line Response of a Cylinder in Oscillatory Flow", *Applied Ocean Research*, Vol. 7 (2), pp. 97–106.

[9] Sumer, B. M., and Fredsøe, J., 1997, "Transverse Vibrations of an Elastically Mounted Cylinder Exposed to an Oscillating Flow", *Journal of Offshore Mechanics and Arctic Engineering*, Vol. 110, pp. 387–394.

[10] Lipsett, A. W., and Williamson, I. D., 1994, "Response of a Cylinder in Oscillatory Flow", *Journal of Fluids and Structures*, Vol. 8 (7), pp. 681–709.

[11] Domenichini, F., 2002, "Quasiperiodicity and Chaos in the Dynamics of an Elastically Mounted Circular Cylinder", *European Journal of Mechanics-B/Fluids*, Vol. 21 (3), pp. 341–354.

[12] Morison, J., Johnson, J., and Schaaf, S., 1950, "The Force Exerted by Surface Waves on Piles", *Journal of Petroleum Technology*, Vol. 2 (5), pp. 149–154.

[13] Anagnostopoulos, P., and Iliadis, G., 1998, "Numerical Study of the Flow Pattern and the In-Line Response of a Flexible Cylinder in an Oscillating Stream", *Journal of Fluids and Structures*, Vol. 12 (3), pp. 225–258.

[14] Taheri, E., Zhao, M., Wu, H., and Tong, F., 2020, "Numerical Investigation of Streamwise Vibration of an Elastically Mounted Circular Cylinder in Oscillatory Flow", *Ocean Engineering*, Vol. 209, p. 107300.

[15] McConnell, K. G., and Jiao, Q., 1986, "The In-Line Forces Acting on an Elastically Mounted Cylinder Oscillating in Still Water", *Experimental Mechanics*, Vol. 26 (1), pp. 66–70.

[16] Zhao, M., Cheng, L., and An, H., 2012, "Numerical Investigation of Vortex-Induced Vibration of a Circular Cylinder in Transverse Direction in Oscillatory Flow", *Ocean Engineering*, Vol. 41, pp. 39–52.

[17] Zhao, M., Pearcey, T., Cheng, L., and Xiang, Y., 2017, "Three-Dimensional Numerical Simulations of Vortex-Induced Vibrations of a Circular Cylinder in Oscillatory Flow", *Journal of Waterway, Port, Coastal, and Ocean Engineering*, Vol. 143 (4), p. 04017007.

[18] Harlow, F. H., and Welch, J. E., 1965, "Numerical Calculation of Time-Dependent Viscous Incompressible Flow of Fluid with Free Surface", *The Physics of Fluids*, Vol. 8 (12), pp. 2182–2189.

[19] Baranyi, L., 2008, "Numerical simulation of flow around an orbiting cylinder at different ellipticity values", *Journal of Fluids and Structures*, Vol. 24 (6), pp. 883–906.

[20] Konstantinidis, E., Dorogi, D., and Baranyi, L., 2021, "Resonance in Vortex-Induced In-Line Vibration at Low Reynolds Numbers", *Journal of Fluid Mechanics*, Vol. 907, p. A34.

[21] Singh, S., and Mittal, S., 2005, "Vortex-Induced Oscillations at Low Reynolds Numbers: Hysteresis and Vortex-Shedding Modes", *Journal of Fluids and Structures*, Vol. 20 (8), pp. 1085–1104.

[22] Govardhan, R., and Williamson, C., 2006, "Defining the Modified Griffin Plot in Vortex-Induced Vibration: Revealing the Effect of Reynolds Number Using Controlled Damping", *Journal of Fluid Mechanics*, Vol. 561, pp. 147–180.